Bulletin of the Seismological Society of America, Vol. 99, No. 3, pp. 1521–1537, June 2009, doi: 10.1785/0120080193

Numerical Study of Ground-Motion Differences between Buried-Rupturing and Surface-Rupturing Earthquakes

by Arben Pitarka,* Luis A. Dalguer, Steven M. Day, Paul G. Somerville, and Kazuo Dan

Abstract Recent ground-motion observations suggest that surface-rupturing earthquakes generate weaker near-fault ground motion than buried earthquakes. This difference is significant in the period range of 0.3–3 sec. Contributing factors to this phenomenon may include the effect of fault zone weakness at shallow depth on rupture dynamics and rupture directivity during earthquakes.

We present results from numerical experiments of spontaneous dynamic rupture and near-source ground-motion simulations of surface rupturing and buried earthquakes and discuss mechanisms for the observed ground-motion differences. The surface-rupturing earthquake is modeled with a shallow zone of 5 km thickness containing areas of negative stress drop (within the framework of the slip-weakening friction model) and lower rigidity. Surface-rupturing models with this weak zone generate lower amplitude ground velocity than do models without this modification.

Observed ground-motion differences between surface and buried events are qualitatively reproduced by imposing higher stress drop in the buried earthquakes than in the surface earthquakes, combined with introducing a deeper rupture initiation for buried rupture, enhancing upward rupture-directivity effects for the latter events. In the context of our simplified model parameterization, then, the observed differences in ground motion could arise from combined effects of relative weakness of the shallow layer of faults, the relatively larger stress drops of buried ruptures, and a tendency of near-fault sites to record strong upward directivity from buried ruptures.

Introduction

Kinematic rupture models used in numerical prediction of ground motion are not directly tied to physical constraints on the causative source physics. This may lead to a crude representation of the observed ground-motion variability caused by the complexities in the fault rupture process. One important observation that needs to be accommodated by the rupture models used in strong ground-motion simulations is the difference in ground-motion characteristics between buried and surface-rupturing earthquakes.

As shown in Figure 1 at short and intermediate periods (0.3–3.0 sec), the near-fault ground motions at selected stations recorded during earthquakes that produce large surface rupture are systematically weaker than the near-fault ground motions from earthquakes whose ruptures are confined to the subsurface (Somerville, 2003). In particular, the recent Kocaeli, Turkey, and Chi-Chi, Taiwan, earthquakes have surprisingly weak ground motion in the period range 0.1–2.0 sec, about 40% weaker than those of empirical ground-motion models. Figure 2 shows event terms (station- and distance-averaged residuals relative to the empirical model of Abrahamson and Silva, 1997) for sets of surface-rupture (top) and buried-rupture (bottom) earthquakes, respectively. The unit line represents the Abrahamson and Silva (1997) ground-motion empirical model, and lines above the unit line indicate that the event's ground motions on average exceed the model. The ground motions of buried-rupture earthquakes are systematically stronger than those of the surface-rupturing earthquakes over a wide period range. This phenomenon is not region dependent because the recorded data used in the analyses are from crustal earthquakes in different regions around the world (Kagawa *et al.*, 2004). These observations led to the inclusion of depth to top of rupture as a source parameter in most of the Next Generation of Attenuation (NGA) ground-motion prediction models that were published in a special issue of the journal *Earthquake Spectra* (Power *et al.*, 2008).

When analyzing the kinematic rupture models of several earthquakes, Kagawa *et al.* (2004) found that earthquakes with surface rupture have asperities (regions of large slip) at depths shallower than 5 km, while earthquakes with buried rupture

*Now at Quantum Technology Sciences, Incorporated, 1980 North Atlantic Ave., Cocoa Beach, Florida 32931; apitarka@qtsi.com.

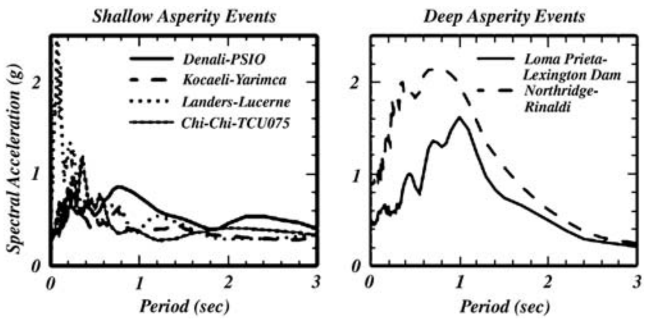

Figure 1. Near-fault response spectra of recent large earthquakes recorded at selected stations. Left: four earthquakes, M_w 7.2 to 7.9, with shallow asperities and large surface faulting. Right: two earthquakes, M_w 6.7 and 7.0, with deep asperities and no surface faulting. Legend indicates the names of each earthquake and associated station, respectively (Somerville and Pitarka, 2006).

have asperities that are usually deeper than 5 km. Further, they found that surface-rupturing earthquakes have larger rupture area and hence lower stress drop than buried-rupture earthquakes. Their analyses show that, compared with shallow asperities, deep asperities have on average three times larger stress drop as well as two times larger peak slip velocity. Although limited to long periods, these kinematic rupture models of past earthquakes suggest that the cause of the observed differences in ground-motion amplitude and frequency content produced by surface and buried rupture is mainly due to differences in fault rupture dynamics in the shallow regions of the crust, compared with rupture at greater depths.

If frictional properties are distinct in the shallow part of faults, the consequent effects on rupture dynamics may play a role in controlling these differences (e.g., Day and Ely, 2002; Pitarka *et al.*, 2005). Therefore, in this article we carry out numerical experiments that consider a weak shallow layer of faulting in combination with depth variations in stress drop and hypocenter location and then compare ground-motion results from surface rupturing and buried earthquakes in the context of this model.

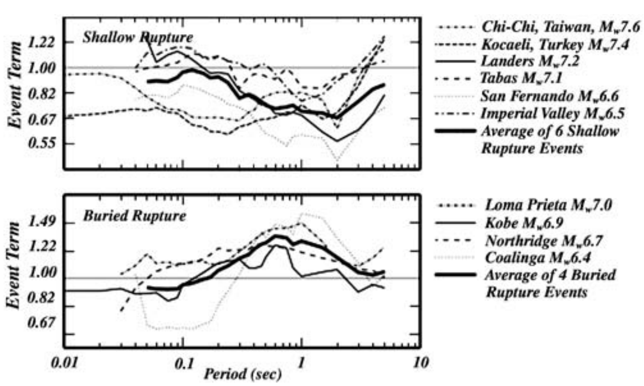

Figure 2. Comparison of response spectral amplitude of individual earthquakes having surface rupture (top) and buried rupture (bottom), averaged over recording sites and at all distances, with the amplitude of the average earthquake as represented by the model of Abrahamson and Silva (1997), represented by the unit line that accounts for magnitude, closest distance, and recording site category. The event terms (residuals) are shown as the ratio of the event to the model (Somerville, 2003).

Shallow-Weak Layer

Brune and Anooshehpoor (1998) discuss the physical properties of the shallow-weak layer and describe its effect in reducing high-frequency seismic energy during shallow faulting. By weak layer we mean a shallow zone of reduced dynamic stress drop resulting from (1) low initial shear stress levels at shallow depth, (2) frictional properties distinct from those at deeper levels, or both. Low initial shear stress results, for example, when normal stress at shallow depth is limited to the weight of the overburden (as in normal faulting environments) or when the fault zone contains a layer of relatively incompetent fault gouge that is not able to maintain large shear stresses (e.g., Marone, 1998). A thick gouge layer may also have frictional behavior in which the resisting force during sliding increases with the slip velocity (Marone and Scholz, 1988). This so-called velocity strengthening behavior tends to reduce the particle velocity and rupture speed. A weak layer might also be expected in the presence of thick surface deposits of sediments, and wave propagation and absorption effects in such deposits might reinforce the dynamic effects, that is, by preferentially absorbing high-frequency waves and amplifying lower frequency waves.

The presence of velocity-strengthening friction at shallow depths has been observed in laboratory experiments where the rock friction at low normal stress exhibits velocity-strengthening behavior (e.g., Shimamoto and Logan, 1981; Marone *et al.*, 1991; Marone, 1998). Also studies of interseismic shallow creep (e.g., Lyons *et al.*, 2002) and shallow post seismic slip of large earthquakes (Marone *et al.*, 1991; Marone, 1998) provide indirect evidence for a velocity-strengthening fault rheology at shallow depths. Moreover, analyses of scaling properties of fracture energy derived from dynamic rupture models of past earthquakes (Mai *et al.*, 2006) show that the fracture energy scales differently for surface rupture than it does for buried rupture. Their study suggests that surface-rupturing earthquakes consume more energy as the rupture expands and reaches the free surface compared with buried-rupture earthquakes.

Scale-model earthquake experiments using foam-rubber blocks by Brune and Anooshepoor (1998) showed that velocity strengthening in a shallow zone suppresses high-frequency components of the slip. Day and Ely (2002) extended the original experimental investigation of Brune and Anooshepoor (1998) to studying the effects of the weak zone on near-fault ground motion. Using a 3D finite difference technique they demonstrated that the foam-rubber experiment can be very well reproduced by rupture dynamic modeling using the slip-weakening friction law (in which the friction coefficient weakens in proportion to slip, up to some critical slip [Dc]) combined with equivalent slip strengthening in the weak zone. Through numerical modeling they analyzed the propagation of rupture through the weak zone in more detail than is available from the laboratory observations alone. The numerical simulations predicted that the weak zone diminishes surface accelerations and velocities out to a fault-normal distance that scales with the weak-zone depth, beyond which there were differing effects on peak acceleration and peak velocity. This result provides insights into finding physical explanations of the difference in ground motion between buried rupturing and surface rupturing.

Pitarka *et al.* (2005) and Somerville and Pitarka (2006) used the results from these studies and numerical simulations of rupture dynamics to suggest a partial explanation for the frequency-dependent difference between observed ground motion from buried and surface rupturing. Their modeling of rupture dynamics using simple models with depth dependent frictional properties suggested a direct link between the significant changes in the rupture dynamics as it propagates through deep and shallow asperities and the frequency content of the generated ground motion. However, their exploratory study was based on a limited number of numerical experiments and simple homogeneous stress models.

In a more rigorous study Dalguer *et al.* (2008) proposed another explanation. They attributed the difference in ground motion between the two types of faulting to the differences in stress-drop distribution, fracture energy, and hypocenter location. These authors calibrated the stress-drop distribution that results in fault ruptures consistent with statistical observations of past earthquakes and inferred that the surface-rupturing earthquakes are characterized by a large area of negative stress drop surrounding the asperities, while buried earthquakes are characterized by nonnegative stress drop. Based on these calibrated dynamic models, they proposed possible mechanisms that satisfy this observed ground-motion difference as follows: buried rupture has hypocenter location below the asperity. This can produce strong directivity of the slip velocity function toward the free-surface. That effect, in addition to low fracture energy during rupture, may be significant in enhancing high-frequency ground motion. On the other hand, surface earthquakes have shallow hypocenter, large fracture energy on the asperities, and enhanced energy absorption due to large areas of negative stress drop in the background area. These characteristics of large earthquakes inhibit severe directivity effects on the slip velocity function directly toward the free surface, reducing the high-frequency ground motion. In essence the calibrated dynamic rupture models of Dalguer *et al.* (2008) and the shallow weak-layer model (e.g., Day and Ely, 2002; Somerville and Pitarka, 2006) are similar in the sense that both assume large enhanced energy absorption areas of negative stress drop for surface rupture. They differ only in the location of such areas; in the shallow-weak-layer model the negative stress-drop area is mainly concentrated within the weak zone in the upper 5 km of the crust, while Dalguer *et al.* (2008) do not restrict the negative stress-drop area to the shallow zone only.

In this study we pursue the concept of shallow weak-layer effect on surface-rupture dynamics and examine the extent to which it explains the observed differences in ground motion between surface- and buried-rupturing events. We improved our original rupture dynamic simulations by using rupture models with stochastic stress drop and extended the analyses to faults with different lengths.

Rupture Model Parameterization

In developing stochastic stress-drop rupture models we followed the work of Andrews (1980), Day (1982), and Oglesby and Day (2002). The fundamental assumption in Andrews' model is that the stress drop is scale invariant, that is, earthquakes of different sizes have the same stress drop. We adopted a stochastic characterization of the spatial complexity of earthquake rupture stress drop in which the stress distribution is described by a power spectral density function in the wavenumber domain, parameterized by two characteristic length scales, along the strike and dip directions, respectively (e.g., Somerville *et al.*, 1999). The spectral decay above the corner wavenumber along the strike and dip directions is proportional to k^{-1} where k is the wavenumber (Andrews, 1980). The spectral decay controls the roughness of the spatial stress distribution. In terms of ground motion k^{-1} spectral stress model is equivalent to the k^{-2} spectral slip model. Both models produce ω^{-2} type near-fault ground motion. Stochastic models described by a power density function have also been used for describing the kinematic slip distribution on the fault (e.g., Somerville *et al.*, 1999; Mai and Beroza, 2002; Lavallee and Archuleta, 2003; Liu *et al.*, 2006) and initial stress (e.g., Ripperger *et al.*, 2008). We assume that the long-wavelength components of the stress drop depend on the regional stress whereas its small-scale fluctuations are caused by the variation of sliding friction on the fault. These spatial stress fluctuations are intended to represent the effect of fault surface random irregularities in generating high-frequency ground motion.

Following Oglesby and Day (2002), both initial shear and normal stress in our models are considered variable in space, but they have the same spatial variation pattern. The key parameter is the relative fault strength that is measured as $S = (\sigma_y - \sigma_o)/(\sigma_o - \sigma_f)$, where σ_y is yield stress, σ_o is initial stress, and σ_f is the sliding frictional stress. In the low-initial stress regions that serve as barriers to the rupture, the relative fault strength is kept higher. In contrast, in the high-initial stress areas that are prone to rupture, S is maintained low. Both conditions are satisfied by a small modification of the assumed initial spatial distribution of the normal stress σ_n^o following the technique of Oglesby and Day (2002)

$$\sigma_n = \sigma_n^o + \varepsilon[\max(\sigma_n^o) - \sigma_n^o],$$

Table 1
Crustal Velocity Model

Layer	V_P (km/sec)	V_S (km/sec)	Density (g/cm^3)	Q
Surface layer	4.8	2.8	2.4	200
Half-space	6.0	3.46	2.67	1000

where σ_n is the normal stress to be used in the dynamic model, σ_n^o is an initial random normal stress, and the maximum of σ_n^o is to be taken over the entire fault. The constant of proportionality ε for the added-in increment is used to control the roughness of the asperities. Finally, the shear and normal stress distributions are scaled to produce a given average stress drop that is invariant in all rupture scenarios. We fixed ε at 0.01. Oglesby and Day (2002) showed that $\varepsilon = 0.01$ produces a rather rough stress-drop distribution. Except for the weak zones for which we applied special conditions explained in subsequent sections, in all models the dynamic friction coefficient is 0.54 and Dc is 30 cm. The static friction coefficient was selected based on the condition that the average value of S should be greater than 2. Under this condition all generated models produced rupture speeds that remain subshear over large areas, except for very small regions where low S may have increased the rupture speed to supershear. The fault is a vertical plane embedded in a heterogeneous space with one horizontal surface layer. The velocity model is described in Table 1.

Rather than limiting rupture to a defined area of the fault by abruptly elevating the friction coefficient at the edges of that area, we instead applied smooth increases in sliding friction and slip-weakening slope around the bottom and lateral fault boundaries, a device intended to roughly mimic a transition to velocity strengthening. This alternative approach avoids the generation of unrealistically large stopping at the fault edges and is facilitated when using stress drop as the random field. The velocity strengthening below the seismogenic zone (depth greater than 15 km) was approximated by linearly increasing the dynamic friction coefficient and the slip-weakening displacement Dc. In this area the stress drop linearly decreases to negative values. This parameterization produces a smooth rupture arrest and a rapid decrease of slip in the transition zone between the brittle frictional sliding and ductile rupture during the earthquake, features that we consider more realistic than those generated by an abrupt strength barrier. The rupture nucleates at a given location in a rectangular area within which we adjust the static friction coefficient so as to bring the strength excess (static shear strength minus initial shear stress) to zero. The simultaneous rupture of the nucleation area creates a pulse-like ground-motion waveform that controls the initial part of the velocity seismogram.

The parameters of our finite source models include the average stress drop, fault strength factor S, and stress-drop correlation lengths along strike and dip directions. The stress correlation lengths are determined based on M_w using the empirical relations of Somerville *et al.* (1999). Other empirical relations based on fault length and fault width can be used as well (e.g., Mai and Beroza, 2002). In simulations of rupture dynamics we used three different stochastic stress-drop models for each of four strike–slip earthquake scenarios with the magnitude M_w ranging from 6.9 to 7.3 and fault length L of 26, 36, 46, and 56 km, respectively (Table 2). For the surface-rupture scenarios the average stress drop was 5 MPa, and hypocentral depth was 7.5 km. For the buried-rupture scenarios, the average stress drop was 7.5 MPa, and the hypocentral depth was 10 km. The upper boundary of the velocity-strengthening transition zone that corresponds to the brittle–ductile boundary in the crust was set to 15 km for all models. Under these assumptions rupture can penetrate a part of the transition zone up to a depth of 17.5 km.

Figure 3 illustrates a stochastic stress model for a surface-rupturing earthquake on a 26 km long fault. Also shown in this figure are the depth variations of normal stress, stress drop, and Dc averaged along the strike of the fault. The station locations for the rupture scenarios considered in this study are presented in Figure 4. We used three linear arrays of stations located on the free surface. The linear arrays are parallel to the fault trace. Their fault distances (distance normal to the fault trace) are 2, 5, and 10 km, respectively.

Rupture Simulations

The spontaneous rupture simulations were performed using a staggered-grid finite difference code (Pitarka, 1999) that uses the staggered-grid split-node method of Dalguer and Day (2007). The grid spacing is 150 m. We used the linear slip-weakening friction law (e.g., Andrews, 1976; Day, 1982). Though it neglects rate dependence and provides only a simplified representation of weakening effects believed to operate at coseismic slip velocities, this parameterization of friction has been successfully used to model fault

Table 2
Rupture Parameters of Surface-Rupturing Scenario Earthquakes

Type of Rupture	Fault Length (km)	Mo (dyne cm)	M_w	Maximum Slip (m)	Surface Slip (m)	Average Slip (m)	Stress Drop (MPa)
Surface	26	2.94×10^{26}	6.9	4.4	2.7	2.4	5.0
Surface	36	4.65×10^{26}	7.1	4.4	2.9	2.6	5.0
Surface	46	6.35×10^{26}	7.2	4.7	3.1	2.8	5.0
Surface	56	8.28×10^{26}	7.3	5.0	3.7	3.0	5.0

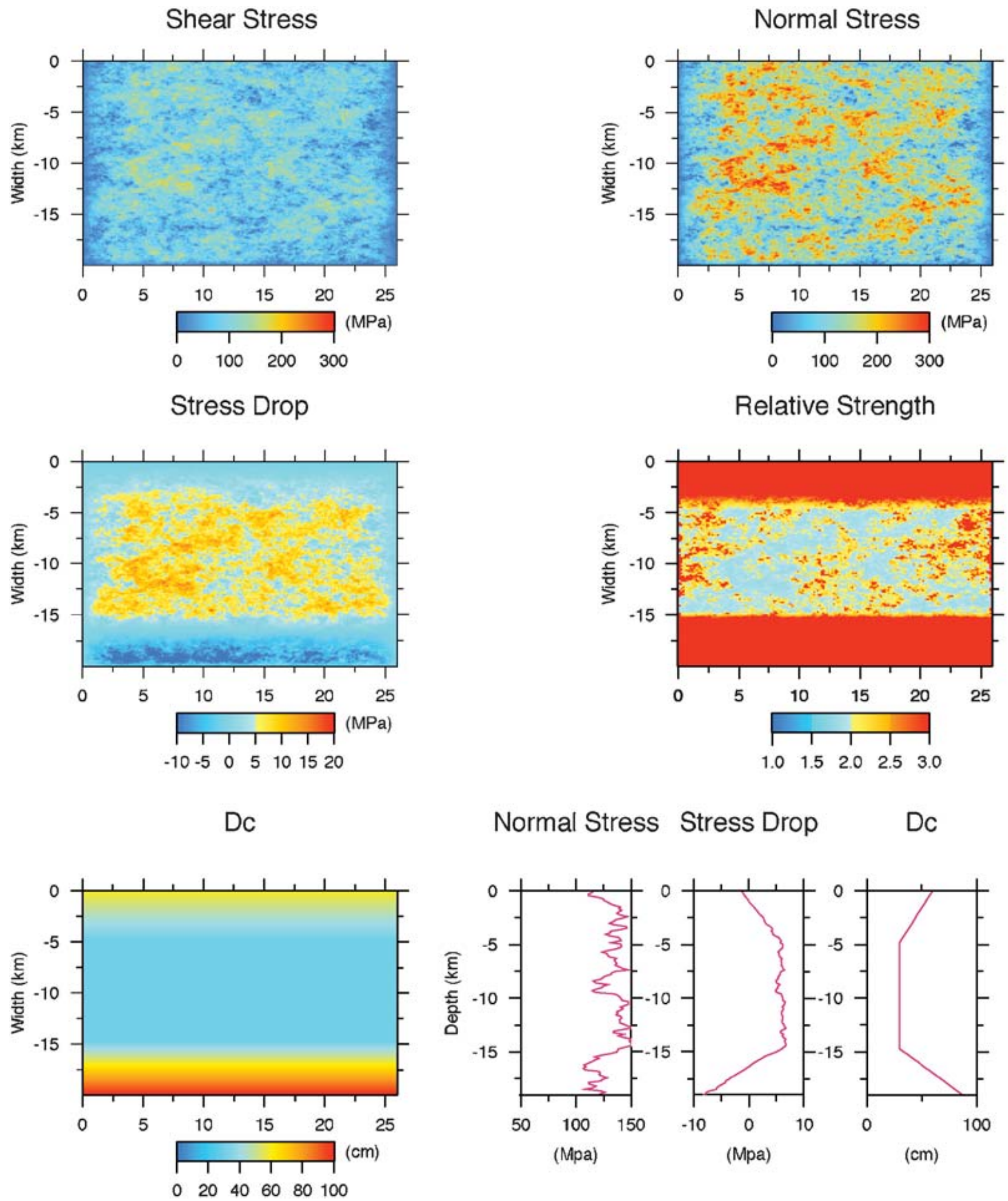

Figure 3. Stochastic stress model for a surface-rupturing earthquake on a 26 km long fault. Lowest panel show depth variation of normal stress, stress drop, and slip-weakening distance Dc, averaged along the strike of the fault. Note that we used a shallow-weak zone between 0 and 5 km and a velocity-strengthening transition zone between 15 and 20 km. Both zones are modeled by linearly decreasing the stress drop and linearly increasing Dc.

slip behavior inferred from seismic recordings of past earthquakes (Ide and Takeo, 1997; Olsen *et al.*, 1997; Day *et al.*, 1998; Dalguer *et al.*, 2001; Ma *et al.*, 2008). In applications to dynamic rupture modeling it has been demonstrated to produce results similar to those obtained with the rate and state friction law (e.g., Okubo, 1989; Cocco and Bizzarri, 2002, 2005; Kaneko *et al.*, 2007). The velocity strengthening in the weak layer was represented in a simplified manner using the slip-weakening friction law. Velocity dependence was not modeled explicitly, but values of the dynamic friction coefficient were set at appropriate elevated levels to yield depth-varying negative stress drop, and slip-weakening offset Dc was increased. Day and Ely (2002) showed that this approximate approach gave simulation results in close agreement with data from scale-model experiments containing a velocity-strengthening strip on the fault surface (Brune and Anooshehpoor, 1998). In the weak layer the slip-weakening distance increases linearly from 30 cm at the bottom of the layer to 100 cm at the free surface. The dynamic friction coefficient follows a linear decay that causes the stress drop to linearly decrease from around 5 MPa at the bottom of the weak layer to negative values at the surface.

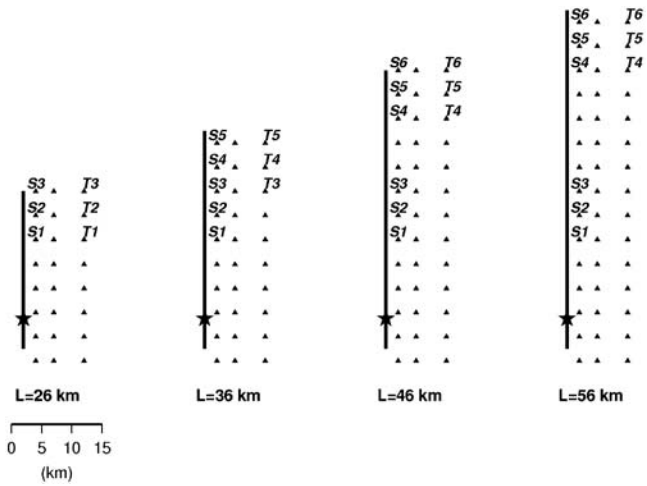

Figure 4. Fault-stations configurations considered in simulating rupture dynamics on vertical faults with different lengths. Triangles are stations, and stars are epicenters. Selected stations whose ground motion is referred to in the text are given a name.

A fast decrease in the stress drop results in a rupture arrest soon after the rupture enters the weak zone. We use this approach in developing buried and surface-rupturing scenarios.

We began by simulating three M 6.9 surface-rupturing earthquakes and one M 6.9 buried-rupture earthquake. We held the seismic moment fixed in these simulations to allow for direct comparison of simulated ground motion among different rupture scenarios. Each earthquake is represented by three scenarios with different stochastic stress-drop distributions. The average stress drop for the surface-rupture models was 5 MPa. In order to produce the target seismic moment, an average stress drop of 7.5 MPa was used for buried-rupture scenarios. This stress-drop adjustment was needed in order to compensate for the smaller rupture area caused by the rupture confinement below the shallow-weak layer. As shown in Figure 5, the three surface-rupturing earthquakes are differentiated by the stress-drop distribution in the 5 km weak-zone layer. In the first model, named the no weak-layer model (top of figure 5), the along-strike averaged stress drop is constant (5 MPa) over the first 15 km depth. In the second model, named the weak layer with low slip strengthening gradient (second line of figure 5), the along-strike averaged stress drop varies linearly from 5 MPa at 5 km depth to approximately -1 MPa at the free surface. And in the third model, named the weak layer with high slip strengthening gradient (third line of figure 5), the along-strike averaged stress drop varies linearly from 5 MPa at 5 km depth to approximately -5 MPa at the free surface. For the buried-rupture model, named the buried fault weak layer with very high slip strengthening gradient (bottom of figure 5), the average stress drop varies linearly from 7.5 MPa at 5 km depth to -20 MPa at the free surface (i.e., such that the rupture remains confined to the subsurface).

Figure 5 shows also the stochastic stress-drop distribution, slip, and rupture time for the models of surface rupturing and buried rupture mentioned previously. The depth variations of along-strike averaged stress drop, slip-weakening distance, and total slip are also shown. The four scenarios result in different slip variations with depth. The slip variation follows closely the variation of stress drop; as would be expected, reducing shallow stress drop correspondingly reduces the shallow slip. However, stress concentrations developed in the high-strength region at depth propagate into the weak zone, producing surface slip even in weak-zone areas of negative stress drop. A similar effect is also seen in the deep weak zone where the slip decreases to zero at a depth of 17.5 km. The absence of a shallow-weak layer (model at the top panel of Fig. 5) causes the largest amount of shallow slip. As expected, this largest slip is mainly due to high stress drop (average 5 MPa) and free-surface effects. This model produces the highest seismic moment. In contrast, the presence of weak layer reduces the shallow slip. The amount of slip in the weak zone, for the second surface-rupturing model, remains significant despite the negative stress-drop values close to the free surface. However, in the third surface-rupturing model with higher negative stress drop, the slip on the weak zone diminishes, reaching minimum values at the free surface. This third model is transitional between buried and surface rupture.

Shallow-Weak Zone Effect on Slip Rate and Ground Motion for Surface-Rupturing Models

Slip rate is a useful measure for comparing rupture models because it directly scales the ground motion generated during an earthquake. In Figure 6 we show the effect of the shallow-weak layer on slip rate by comparing simulated effects of rupture dynamics on three surface-rupturing models. One of the models has no weak layer (top of Fig. 5), and we treat it as a reference model. The other two models have different slip strengthening gradients (second and third line of Fig. 5). The hypocenter is located at a depth of 7.5 km for all three models. Figure 6b shows the time history of the slip rate at receivers in a vertical array located on the fault. Two features of simulated slip velocity are particularly relevant to our investigation of the frequency content of radiated seismic energy during rupture. First, when rupture penetrates into the weak layer, rupture propagation decelerates, the slip rate gets smoother, and its peak reduces gradually toward the free surface, but then at the free-surface, the peak slightly recovers due to the free-surface reflection. This effect of the weak zone on the slip-rate function suggests a reduction of the high frequency ground motion. Second, due to rupture deceleration and delay of reflected pulses from the free surface and stopping phases from the fault edges, the rise time becomes longer in this zone, suggesting a shift to lower frequency content of the ground motion. Figure 6c displays velocity seismograms for each model at stations S3 and T3 (see Fig. 4 for location of stations), showing that the ground-motion amplitude is considerably reduced for models with shallow-weak zone. The sharp pulse due to rupture-directivity,

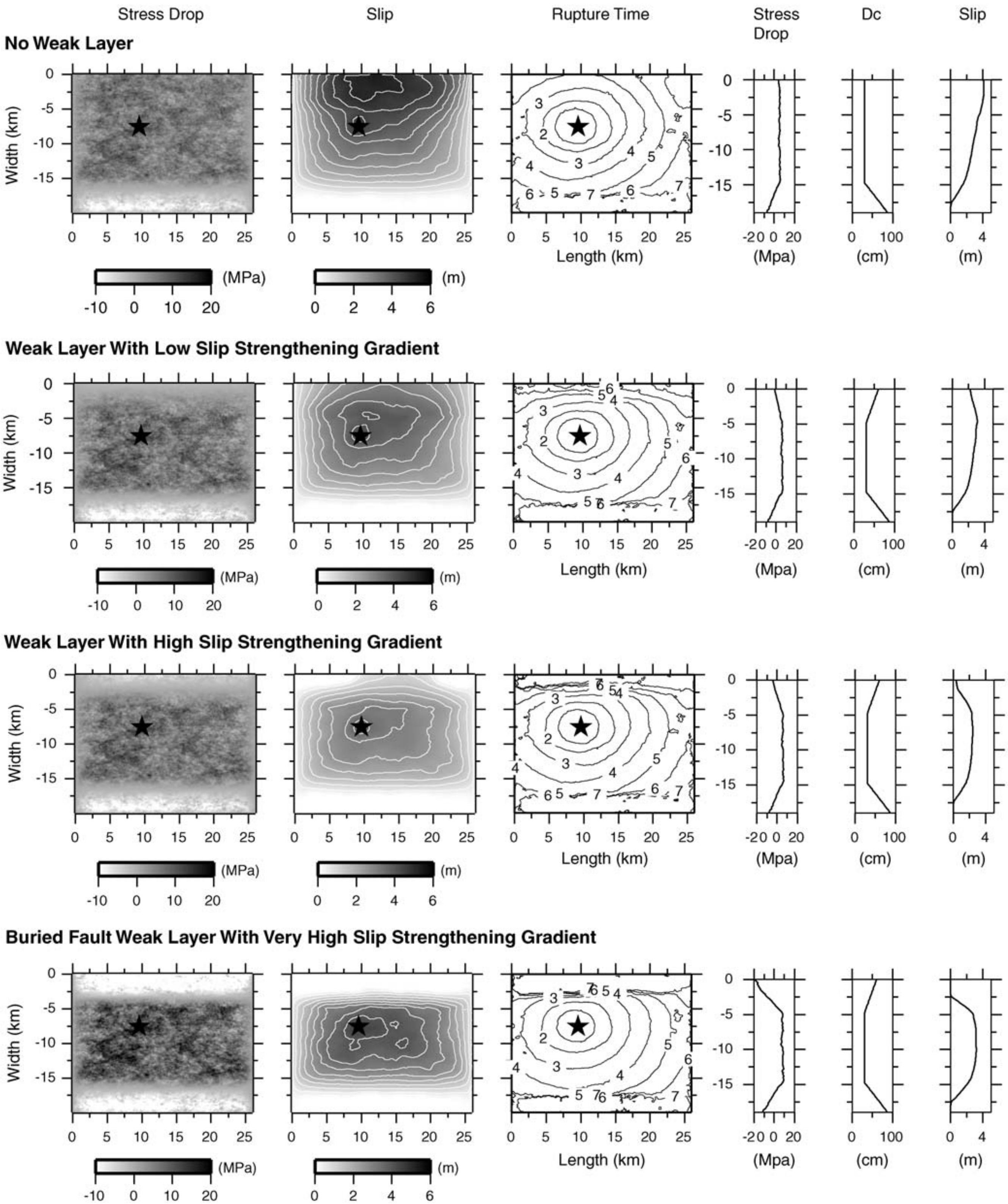

Figure 5. Examples of stochastic stress drop and corresponding calculated slip and rupture time for models of surface rupture and buried rupture. The depth variations of along-strike averaged stress drop, slip-weakening distance, and total slip are shown on the right. The four scenarios result in different slip variations with depth. The slip variation follows the variation of stress drop. Note that the weaker the zone (larger negative stress drop), the smaller the shallow slip.

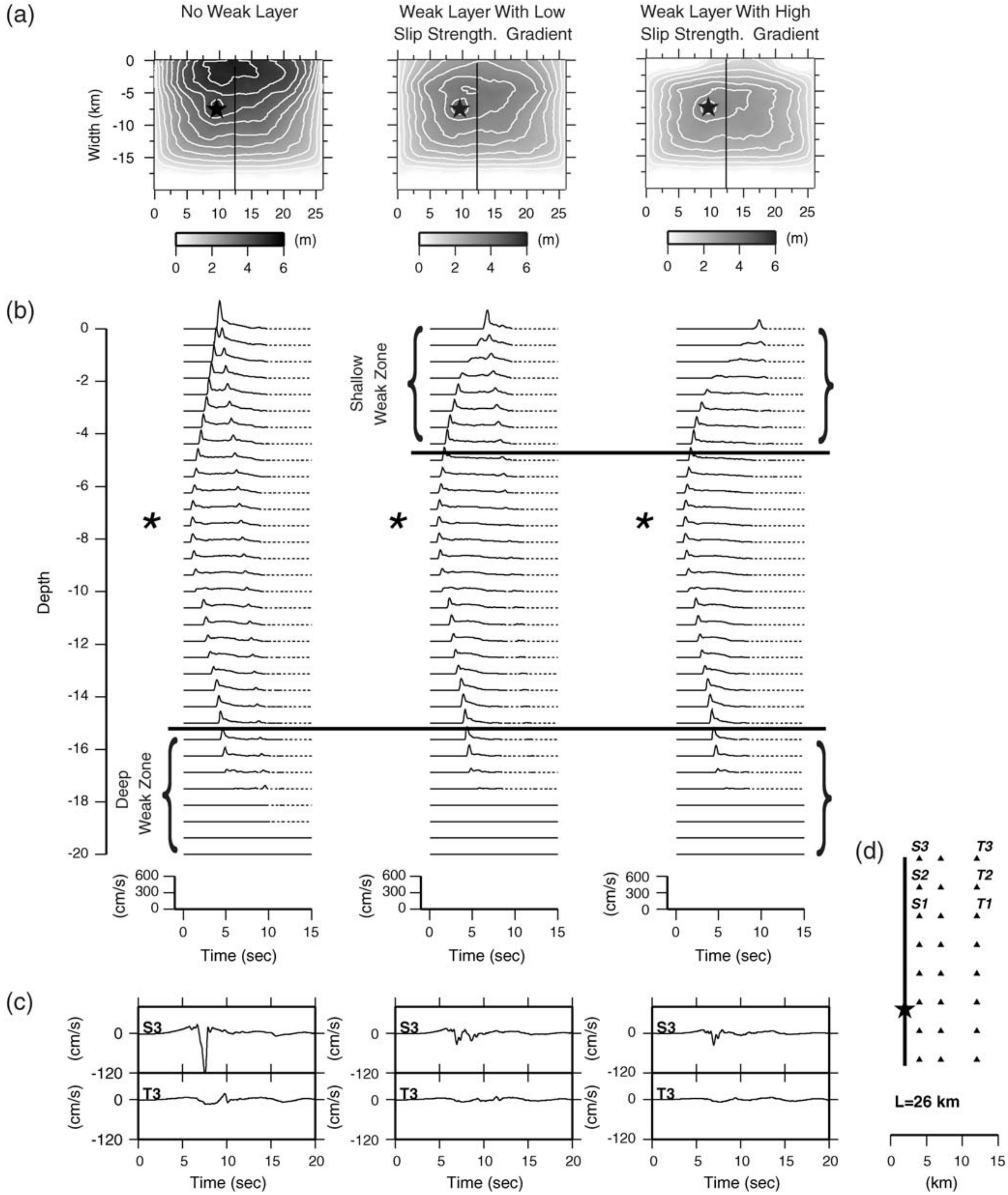

Figure 6. Simulated effects of rupture dynamics on (a) final slip, (b) slip rate, and (c) ground-motion velocity for surface rupturing with no weak layer (left panels), with weak layer with low-rate slip strengthening (middle panels), and with weak high-rate slip strengthening (right panels). (d) Fault-stations configuration. The shallow-weak layer is located between 0 and 5 km. The time history of slip rate is shown for receivers located in a vertical array across the fault, indicated by a thin line on the slip distribution panels. Stars indicate hypocenter location. Note the reduction of slip rate in the shallow-weak zone and corresponding reduction in ground-motion amplitude at stations S3 and T3 for models with shallow-weak layer (middle and right panels).

observed in the model with no weak layer, is not seen in the models with weak zone. The weakest ground motion is generated by the third model, the transitional case mentioned earlier (third line panels in Fig. 5) that also produced the smallest rupture area and smallest average slip.

Slip Rate and Ground Motion from Buried Earthuakes

Now we evaluate slip rate and ground-motion characteristics of buried ruptures. As shown by Dalguer *et al.* (2008), rupture models with deep hypocenter location can produce directivity leading to concentration of the slip rate toward the free surface. This effect may enhance high-frequency ground motion. Here, we test two buried-rupture scenarios with different hypocenter depths but the same average stress drop of 7.5 MPa. In our simulations of buried rupture the rupture's arrest is naturally realized by increasing gradually the negative stress drop in the weak-shallow layer, as explained previously and shown in the bottom panel of Figure 5. Figure 7 displays the final slip distribution, slip-rate time histories, and ground velocities at stations S3 and T3 for both models. As seen in Figure 7b, the model with deeper hypocenter generates the highest peak slip rate, and this is due to the effect of directivity due to upward rupture propagation. As a consequence of this effect, the velocity ground motion produced by the model with deeper hypocenter is stronger (note in Fig. 7c, the sharp pulse at station S3).

Comparison of ground velocity from the surface-rupturing model with shallow-weak zone (Figure 6c) with that from our buried-rupture model (Figure 7c) shows a general bias toward stronger motion from the latter. We compare frequency content in the next section.

Analysis of Ground-Motion Differences between Surface and Buried Rupture

Somerville (2003) investigated the ground-motion difference between surface rupturing and buried-rupture earthquakes by comparing the response spectral amplitude of individual earthquakes averaged over the recording sites with amplitude of the average earthquake as represented by the empirical model of Abrahamson and Silva (1997). Here, we used a similar two-step procedure, but instead of the response spectrum, we used the Fourier spectrum. First, we computed the amplitude spectrum for both types of ruptures by averaging over three realizations of each scenario and over stations with the same fault distance. Then, for each fault distance we computed the ratio between the average spectrum of buried rupture and the average spectrum of surface rupture.

Figure 8 compares the spectral ratios (buried-rupture divided by surface-rupture earthquakes). The surface-rupture earthquakes were computed using models with high-gradient weak layer, low-gradient weak layer, and no weak layer, respectively, and an average stress drop of 5 MPa. The buried-rupture earthquakes were computed using models with a very high-gradient weak layer. The high gradient forced the rupture to stop below the free surface at a depth of 2.5 km. As mentioned earlier, in order to match the seismic moment of buried-rupture scenarios to that of surface-rupture scenarios with weak layer, the average stress drop of buried-rupture scenarios was increased to 7.5 MPa. The spectral ratios are calculated for fault-normal, fault-parallel, and vertical components of ground-motion velocity in the period range of 0.2–10 sec in which the numerical simulations are accurate. As a general observation, the buried-rupture ground motion is stronger on the fault-normal direction only, as is seen comparing Figure 8a with Figure 8b and Figure 8c. For models with weak layer the fault-normal ground motion from buried rupture is higher than that of surface rupture in the period range of 0.7–4 sec and periods shorter than 0.3 sec at fault distances of 2 km and 5 km. Surface-rupture models with low stress-drop gradient in the weak zone produce larger ground motion in the period range 0.3–0.7 sec. This period range broadens to 0.3–2 sec at the fault distance of 10 km. The overall characteristics of the fault-normal ground motion from surface-rupturing earthquakes are also affected by the lateral rupture directivity, enhanced by the shallow slip and wave propagation effects in the low velocity surface layer.

As expected, the surface-rupture scenario without weak layer produces very large surface slip. The resulting ground motion is unrealistically high and much higher than that of buried rupture.

Mai *et al.* (2005) found that most earthquakes have hypocenters located in regions of large slip. However, they did not find any clear association between the hypocentral depth and buried–surface faulting. A few large earthquakes included in their study do indicate that surface-rupturing earthquakes nucleate at shallower depths compared to smaller buried-rupture earthquakes (Mai, personal comm., 2008). The effect of variation in hypocentral depth on buried–surface ratio is shown in Figure 9. In this figure we compare spectral ratios between buried ruptures initiated at depths of 7.5 km (thick line) and 10 km (thin line) and surface rupture initiated at a depth of 7.5 km for fault-normal and fault-parallel components of ground motion. The effect of the hypocentral depth is significant. As explained in the previous section, because of the weak-zone effects on rupture dynamics during surface rupture, and rupture directivity effects enhanced by the deep hypocenter during buried rupture, the buried fault ground motion is in general higher on a broad frequency range for the fault distance of 2 km. This feature slightly changes at the fault distance of 5 km for which buried ruptures produce higher ground motion in the intermediate period range (1–4 sec) only.

The simulation results we have shown so far are for comparisons between surface and buried-rupture earthquakes with the same magnitude and same fault length. The difference between their seismic moments is less

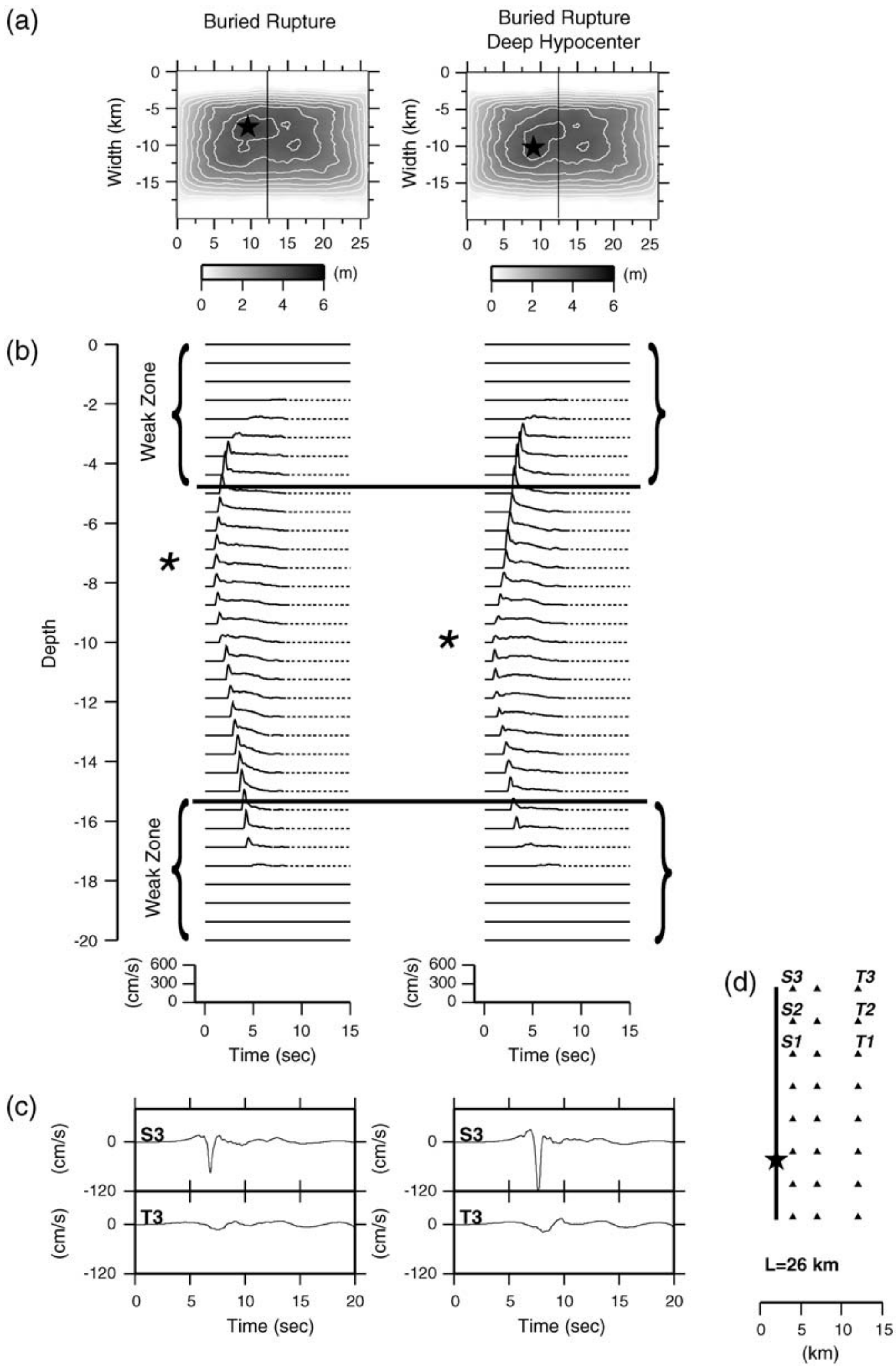

Figure 7. Simulated effects of rupture directivity and weak layer on (a) final dynamic slip, (b) slip rate, and (c) ground-motion velocity for buried rupturing with shallow rupture initiation (left panels) and deep rupture initiation (right panels). (d) Fault-stations configuration. The time history of slip rate is shown for receivers located in a vertical array across the fault, indicated by a thin line on the slip distribution panels. Note the increase in slip-rate amplitude in the upward direction of rupture propagation. For the same stress drop, the model with deep rupture initiation produces larger peak slip rate. Because of the stronger rupture-directivity effect, the corresponding ground-motion pulse at receiver S3 has larger amplitude. The directivity effect is negligible at station T3, which has a fault distance of 10 km.

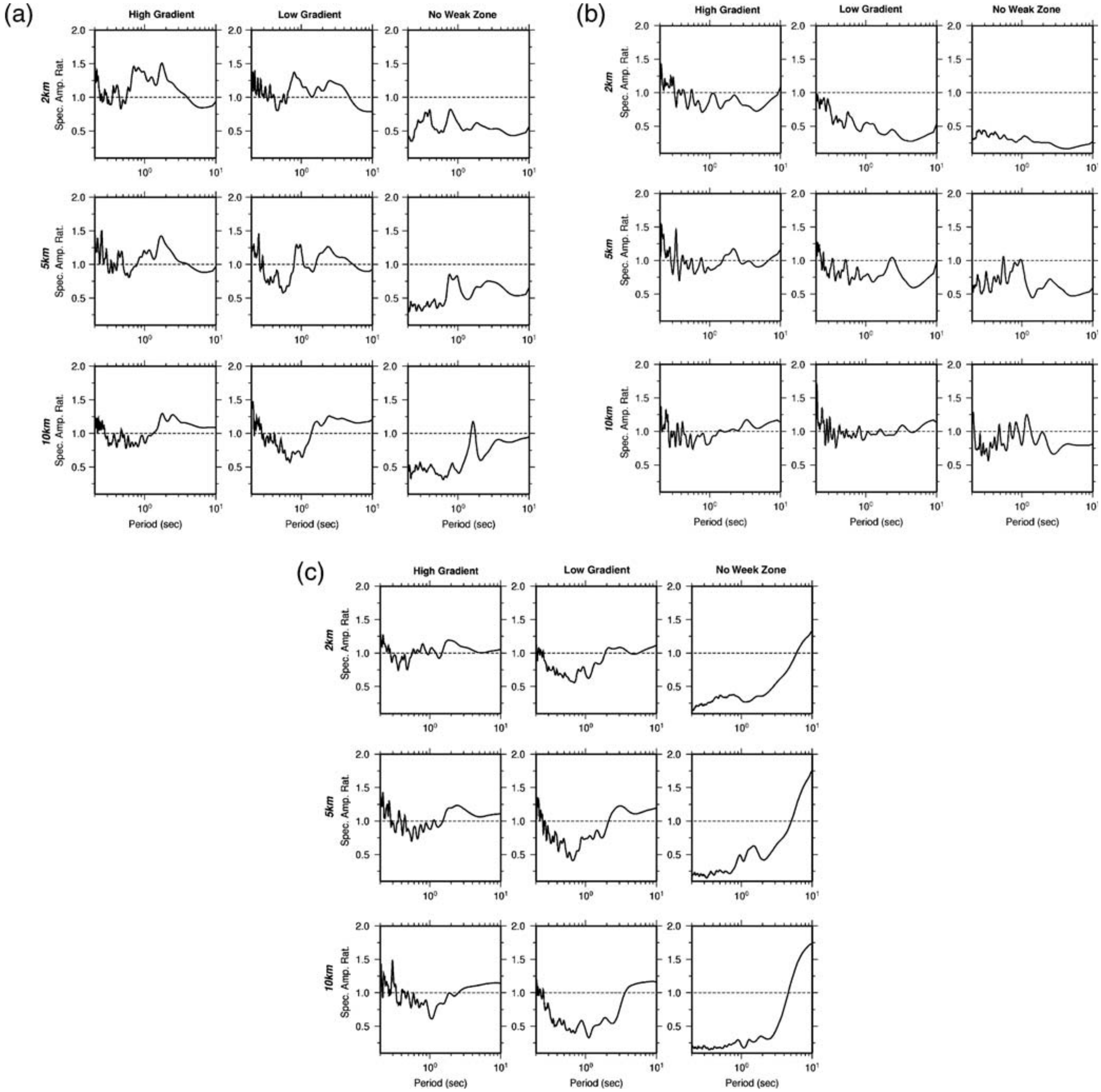

Figure 8. (a) Average spectral ratios of fault-normal ground-motion velocity between buried rupture and surface-rupturing earthquakes calculated at fault distances of 2 km (top panels), 5 km (middle panels), and 10 km (bottom panels). The ground motion for surface-rupturing earthquakes was computed using stress models with high-gradient weak zone (left panels), low-gradient weak zone (central panels), and without weak zone (right panels), respectively. (b) Same as Figure 8a but for fault-parallel component. (c) Same as Figure 8a but for vertical component.

than 6%. We extended our analysis by simulating surface-rupturing earthquakes with fault lengths of 26, 36, 46, and 56 km, respectively. Their corresponding magnitudes M_w are in the range of 6.9–7.3 (Table 2). Figure 10 shows examples of distributions of slip and rupture time obtained for surface-rupture earthquakes with different fault lengths. Note that all rupture realizations have the same hypocentral location and have scale-invariant average stress drop of 5 MPa. The fault and station configurations used in the calculation of near-fault ground motion are shown in Figure 4.

Table 2 summarizes the relation between seismic moment and slip for each scenario. There is a slight increase of peak slip with the fault length while the average slip and surface slip remain approximately the same for all considered magnitudes. These characteristics are compatible

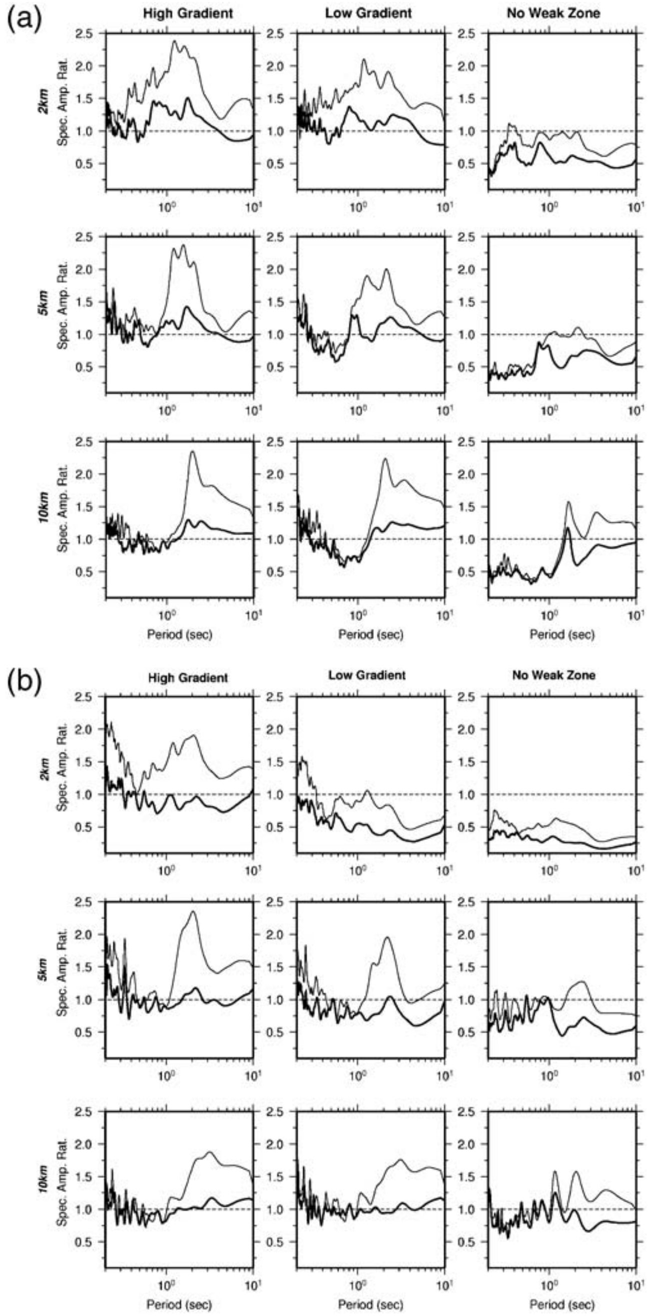

Figure 9. (a) Spectral ratios of fault-normal ground-motion velocity between buried-rupturing earthquakes initiated at 7.5 km (thick line) and 10 km (thin line) depths and surface-rupturing earthquakes initiated at 7.5 km, calculated at fault distances of 2 km (top panels), 5 km (middle panels), and 10 km (bottom panels). The ground motion for surface-rupturing earthquakes was computed using stress models with high-gradient weak zone (left panels), low-gradient weak zone (central panels), and no weak zone (right panels), respectively. (b) Same as Figure 9a but for fault-parallel component.

with the observed slip-length scaling of large earthquakes. As will be shown later, our modeling technique produces ground motion that saturates with magnitude, a distinctive trend manifested in empirical models of moderate size strikes-lip earthquakes. This feature is a consequence of the deep weak zone used in our dynamic rupture models that allows the development of coseismic slip with long rise time at depths below 15 km. The deep weak zone represents the brittle ductile transition at the base of the seismogenic zone (e.g., Das and Scholz, 1983; King and Wesnosky, 2007; Hillers and Wesnosky, 2008).

The simulated ground motion at near-fault stations from surface rupturing of long faults is characterized by a large variation in distance along the fault away from the epicenter (D). This variation is caused by the cumulative effect of small-scale stress-drop heterogeneities along the rupture path and rupture interaction with the free surface. Obviously, the averaging of buried–surface spectral ratio over all stations may obscure spatially varying characteristics of interest. For this reason we calculated the average spectral ratio using stations with distance D covering three ranges, $D < 20$ km, 20 km $< D < 30$ km, and $D > 30$ km, respectively. The results for shallow and deep buried-rupture initiations are shown in Figure 10. From this figure it is clear that for D shorter than 20 km, the spectral ratio between buried and surface rupture is independent of the fault length.

At a fault distance of 2 km the deep buried-rupture earthquakes produce stronger ground motion for periods up to 3 sec. In contrast they produce weaker ground motion at periods longer than about 3 to 5 sec (Fig. 11a). The period range of larger amplitude narrows to about 1–3 sec for fault distances of 5 and 10 km. Also at these distances the ground motion from buried-rupture earthquakes becomes weaker in the short period range of 0.3–0.7 sec. The ground-motion amplitude from buried rupture increases when the hypocentral depth increases. It is obvious that the upward directivity in the buried-rupture earthquakes plays a crucial role at producing larger ground motion at short and intermediate periods. These trends also remain noticeable in the D range between 20 and 30 km (Fig. 11b). For D greater than 30 km and considered fault distances, the ground motion from surface-rupturing earthquakes is larger than that of buried-rupturing earthquakes (Fig. 11c).

The variation of the ground-motion characteristics as a function of D and fault length is illustrated in Figure 12. In this figure we show acceleration response spectra calculated at selected stations. Our numerical simulations predict that for small D and very near to the fault, the ground motion from buried rupture is higher than that from surface rupture for all considered periods, independently of the fault length of surface rupture. The effect of fault length becomes important at larger D (over 30 km) and near-fault locations where the ground motion from surface rupture is higher at long periods but still comparable with that of the buried rupture. Finally, at 10 km from the fault the surface-rupture ground motion from long faults (e.g., $L = 56$ km) becomes larger at all periods. Our simulation suggests that at this distance the effect of the shallow-weak layer during surface rupture and the effect of rupture directivity during buried rupture are both small. Using a simpler stress model Day and Ely (2002) found similar effects. Their numerical experiments suggest

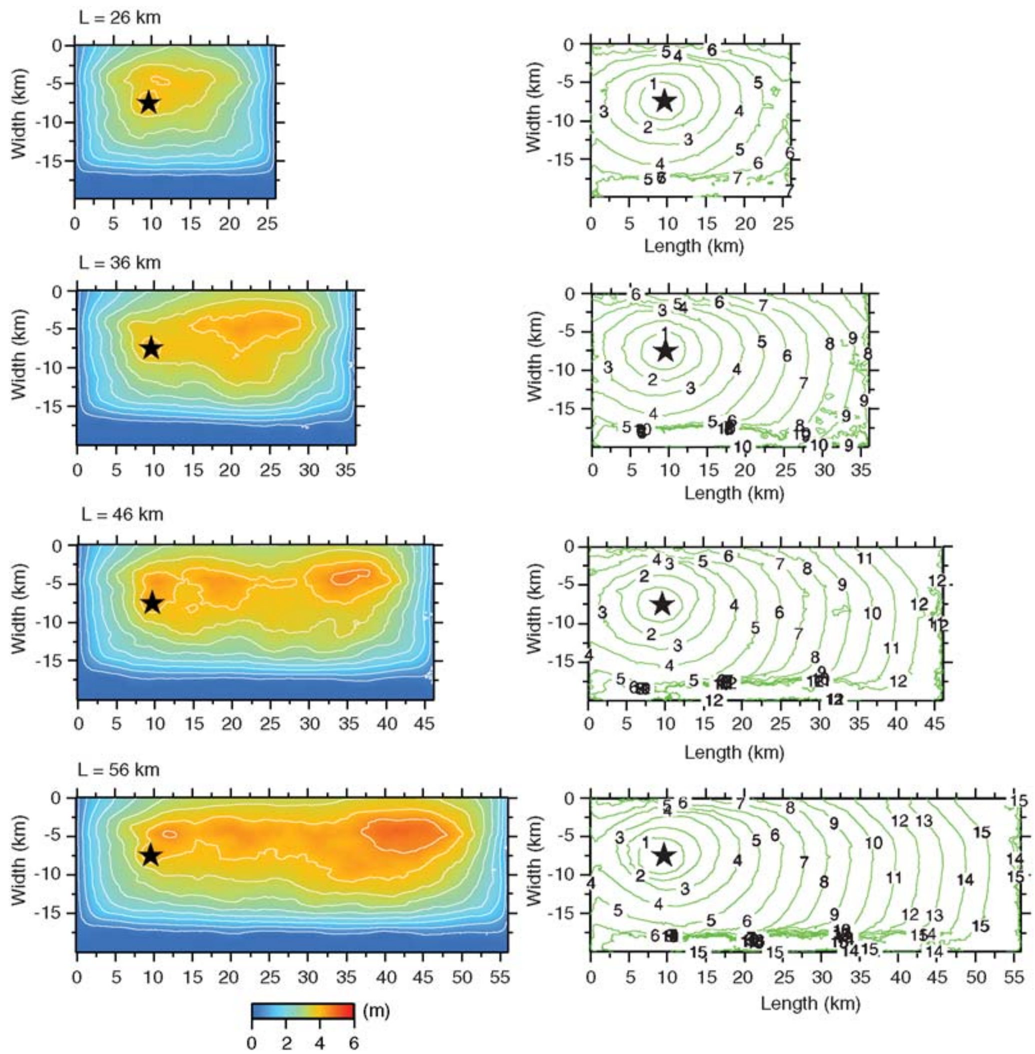

Figure 10. Selected distributions of slip and rupture time obtained for surface-rupture earthquakes with different fault lengths L. L is indicated on top of each panel. Note that all rupture realizations have the same hypocentral location and average stress drop of 5 MPa. Stars indicate the hypocenter location.

that at fault distances larger than the weak zone depth, the effect of the weak zone is small. It can be argued that some of the spatial features of difference in ground motion found in this study are model related. They strongly depend on the stress drop and friction characteristics and width of the weak-zone. We are unable to confirm this finding using available recorded ground-motion data. The spatial distribution and small number of available stations used by Somerville (2003) to demonstrate the difference between surface and buried rupturing, shown in Figure 2, prevented us from performing analyses of difference in recorded ground motion as a function of fault distance. Further investigations using data from recent moderate and large earthquakes are needed.

Conclusions

The effect of the weak zone on rupture dynamics has already been established through foam-rubber laboratory experiments (Brune and Anooshehpoor, 1998) and numerical simulations (e.g., Day and Ely, 2002; Pitarka *et al.*, 2005; Somerville and Pitarka, 2006; Kaneko *et al.*, 2007). In this article we incorporate this weak zone in our surface-rupturing models to investigate ground-motion differences between small, buried earthquakes and large, surface-rupturing earthquakes.

Surface-rupturing earthquakes of strike-slip faults with different lengths are modeled assuming a 5 km thick weak surface layer representing both a weak fault zone and shallow sedimentary deposits in the crust. Ground-motion comparisons between surface-rupturing models, with and without weak zone, shows that the weak-zone layer model generates smoother, lower-amplitude ground velocity due to the reduction of slip rate in the weak-zone fault area.

Our modeling results show that the effects of the weak layer during surface rupturing, combined with effects of upward rupture directivity and larger stress drop in buried

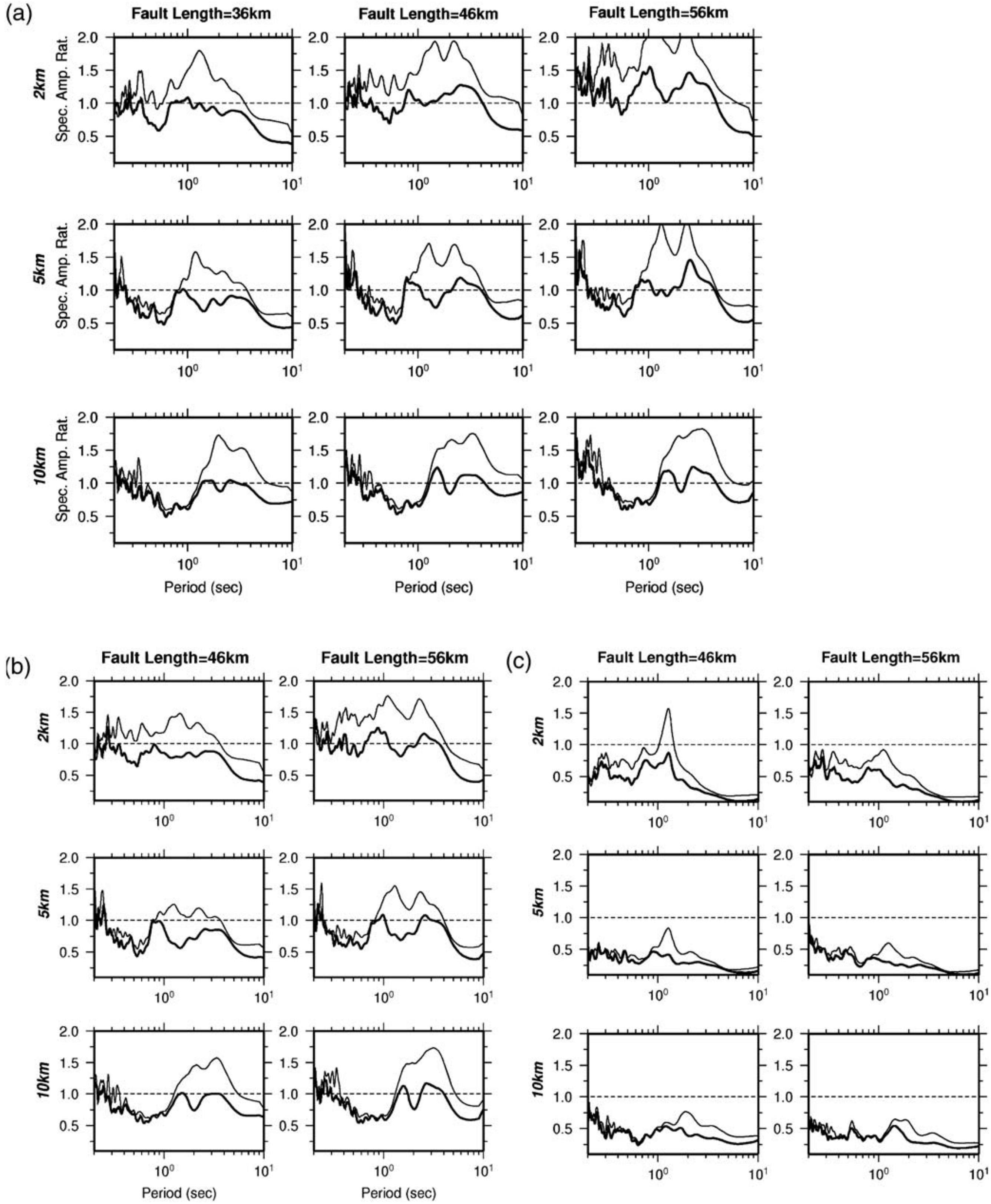

Figure 11. (a) Spectral ratios of fault-normal ground-motion velocity between buried-rupture earthquakes with 26 km fault length and surface-rupturing earthquakes with fault lengths of 36, 46, and 56 km, respectively, averaged over stations with distance along the fault away from the epicenter (*D*) less than 20 km. The buried rupture was initiated at 7.5 km depth (thick line) and 10 km depth (thin line). (b) Same as Figure 11a but for stations with *D* between 20 and 30 km. (c) Same as Figure 11a but for stations with *D* greater than 30 km.

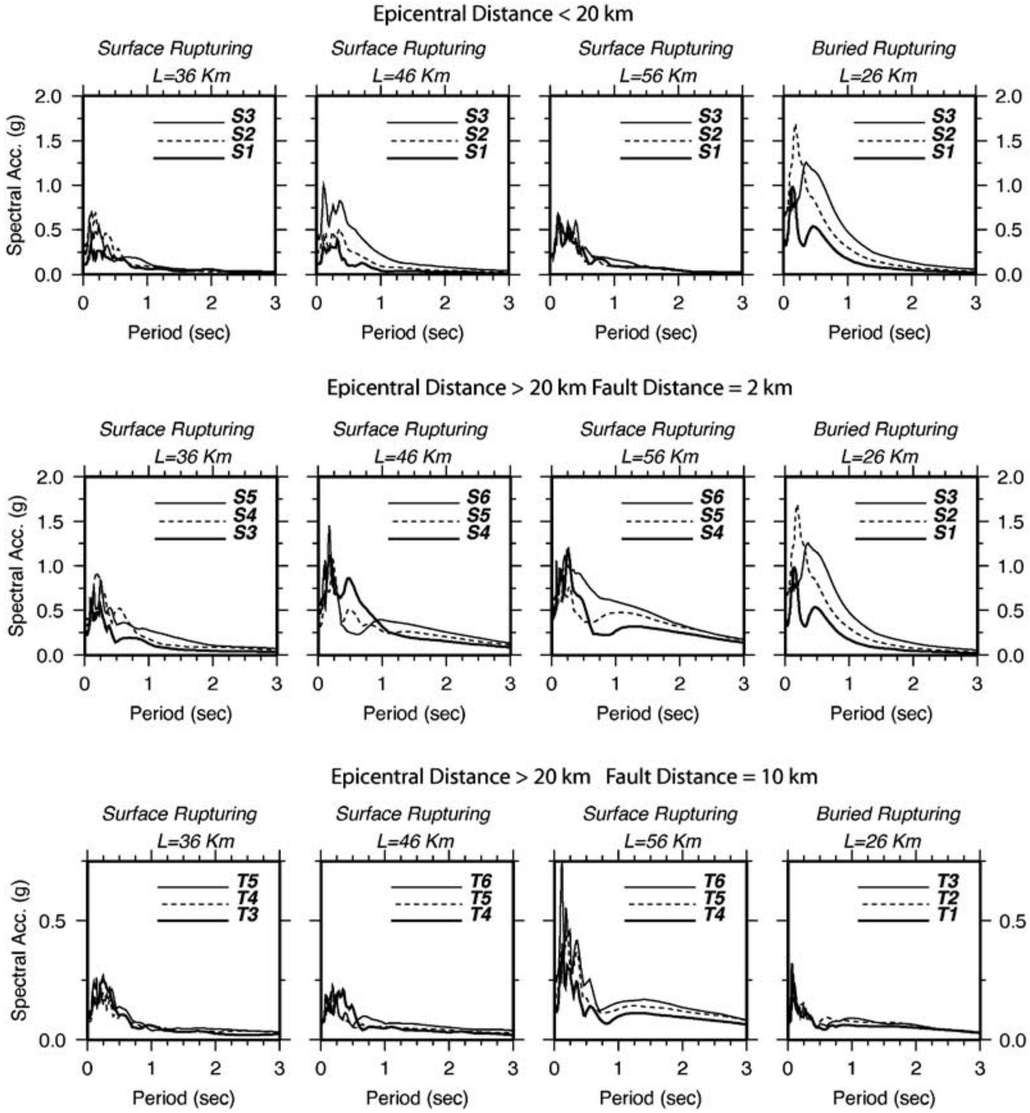

Figure 12. Fault-normal acceleration response spectra for different fault lengths and types of rupture. The spectra are calculated at selected stations with distance along the fault away from the epicenter (D) less than 20 km (top panels), with D greater than 20 km and fault distance 2 km (middle panels), and with D greater than 20 km and fault distance 10 km (bottom panels). The station locations are shown in Figure 4. Note the relatively large amplitude for buried rupture (right panels) compared to surface-rupturing earthquakes with larger magnitude. The type of rupture and fault length L are indicated on top of each panel.

rupturing, may cause a significant contrast in frequency content of ground motion between buried and surface-rupturing earthquakes of strike-slip faults. Higher stress drop and deep rupture initiation during buried earthquakes were found to be key factors in ground-motion amplification in the period range 0.2–3 sec at sites very close to the fault. In contrast, as a result of the weak-zone effect, the ground motion from shallow-slip surface-rupturing earthquakes is greatly reduced in the same period range. These two opposing effects make the ground motion from small buried earthquakes larger than that from large surface-rupturing earthquakes. The period range in which this difference is significant narrows to 0.8–3 sec for fault distances of 5 km and longer. We expect that the opposing effects of upward rupture directivity and weak layer are also significant for dip-slip faulting. Therefore, our arguments used in explaining the difference between buried and surface faulting could also be used for earthquakes on dip-slip faults.

Our simulation suggests that the difference in frequency content of ground motion from buried and surface rupture has limited spatial extent. The upward directivity effect during buried-rupture earthquakes is significant only in a narrow region above the rupture area. This turns out to be the controlling factor of the spatial extent of the simulated contrast in frequency content between the two types of rupture. We found that at distances along the fault and away from epicenter that are smaller than 30 km and fault distances smaller than 10 km, the ground motion from small buried-rupture earthquakes is larger than the ground motion from surface-rupturing earthquakes. In general, beyond these distances the ground motion from surface-rupturing earthquakes is larger. The cutoff distances found here are model dependent. Indeed, the relative area of the shallow-weak zone with respect to the total fault area; and therefore, its effect on ground motion decreases when the fault length increases. Consequently, its relative effect in reducing the ground-motion amplitude decreases with the fault length. This limited spatial extent of the buried–surface spectral difference suggested by our rupture models needs to be validated against observations.

Data Resources

Some plots were made using the Generic Mapping Tools version 4.2.1 (www.soest.hawaii.edu/gmt; Wessel and Smith, 1998; last accessed January 2008).

Acknowledgments

We thank the associate editor David Oglesby and two anonymous referees for helpful comments that improved this manuscript. This work was supported by the U.S. Geological Survey (USGS), Cooperative Agreement Number 06HQGR0043 and the Southern California Earthquake Center (SCEC). SCEC is funded by the National Science Foundation (NSF) Cooperative Agreement Number EAR-0106924.

References

Abrahamson, N. A., and W. J. Silva (1997). Empirical response spectral attenuation relations for shallow crustal earthquakes, *Seism. Res. Lett.* **68,** 94–127.

Andrews, D. J. (1976). Rupture velocity of plane-strain shear cracks, *J. Geophys. Res.* **81,** 5679–5687.

Andrews, D. J. (1980). A stochastic fault model, 1, static case, *J. Geophys. Res.* **78,** 3867–3877.

Bizzarri, A., and M. Cocco (2005). 3D dynamic simulations of spontaneous rupture propagation governed by different constitutive laws with rake rotation allowed, *Annals of Geophysics.* **48,** no. 2, 288–299.

Brune, J. N., and A. Anooshehpoor (1998). A physical model of the effect of a shallow weak layer on strong ground motion for strike-slip ruptures, *Bull. Seismol. Soc. Am.* **88,** 1070–1078.

Cocco, M., and A. Bizzarri (2002). On the slip-weakening behavior of rate and state dependent constitutive laws, *Geophys. Res. Lett.* **29,** doi 10.1029/2001GL013999.

Dalguer, L. A., and S. M. Day (2007). Staggered-grid split nodes method for spontaneous rupture simulation, *J. Geophys. Res.* **112,** B02302, doi 10.1029/2006JB004467.

Dalguer, L. A., K. K. Irikura, J. Riera, and H. C. Chiu (2001). The importance of the dynamic source effects on strong ground motion during the 1999 Chi-Chi (Taiwan) earthquake: Brief interpretation of the damage distribution on buildings, *Bull. Seismol. Soc. Am.* **95,** 1112–1127.

Dalguer, L. A., H. Miyake, S. M. Day, and K. Irikura (2008). Surface-rupturing and buried dynamic rupture models calibrated with statistical observations of past earthquakes, *Bull. Seismol. Soc. Am.* **98,** 1147–1161.

Das, S., and C. Scholz (1983). Why large earthquakes do not nucleate at shallow depth, *Nature* **305,** 621–623.

Day, S. M. (1982). Three-dimensional simulation of spontaneous rupture: The effect of nonuniform prestress, *Bull. Seismol. Soc. Am.* **72,** 1881–1902.

Day, S. M., and G. P. Ely (2002). Effect of a shallow weak zone on fault rupture: Numerical simulation of scale-model experiments, *Bull. Seismol. Soc. Am.* **92,** 3006–3021.

Day, S. M., G. Yu, and D. J. Wald (1998). Dynamic stress changes during earthquake rupture, *Bull Seismol. Soc. Am.* **88,** 512–522.

Hillers, G., and S. G. Wesnousky (2008). Scaling relations of strike-slip earthquakes with different slip-rate dependent properties, *Bull Seismol. Soc. Am.* **98,** 1085–1101.

Ide, S., and M. Takeo (1997). Determination of constitutive relations of fault slip based on seismic wave analyses, *J. Geophys. Res.* **102,** 27379–27391.

Kagawa, T., K. Irikura, and P. Somerville (2004). Differences in ground motion and fault rupture process between surface and buried rupture earthquakes, *Earth Planets Space* **56,** 3–14.

Kaneko, Y., N. lapusta, and J-P. Ampuero (2007). Spectral-element modeling of spontaneous earthquake rupture on rate and state faults: Effects of velocity-strengthening friction at shallow depths, *J. Geophys. Res.* **113,** B09317, doi 10.1029/2007JB005553.

King, G. C. P., and S. G. Wesnousky (2007). Scaling of fault parameters for continental strike-slip earthquakes, *Bull Seismol. Soc. Am.* **97,** 1833–1840.

Lavallee, D., and R. Archuleta (2003). Stochastic modeling of slip spatial complexities for the 1979 Imperial valley, California, earthquake, *Geophys. Res. Lett.* **30,** no. 5, 1245, doi 10.1029/2002GL015839.

Liu, P., R. Archuleta, and S. H. Hartzell (2006). Prediction of broadband ground motion time histories: Frequency method with correlation random source parameters, *Bull. Seismol. Soc. Am.* **96,** 2118–2130, doi 10.1785/0120060036.

Lyons, S. N., Y. Bock, and D. T. Sandwell (2002). Creep along the Imperial fault, southern California, from GPS measurements, *J. Geophys. Res.* **107,** doi 10.1029/2001JB000763.

Ma, S., S. Custodio, R. Archuleta, and P. Liu (2008). Dynamic modeling of the 2004 M_w 6.0 Parkfield, California, earthquake, *J. Geophys. Res.* **113,** B02301, doi 10.1029/2007JB005216.

Mai, P. M., and G. C. Beroza (2002). A spatial random field model to characterize complexity in earthquake slip, *J. Geophys. Res.* **107,** no. B11, 2308, doi 10.1029/2001JB000588.

Mai, P. M., P. Spudich, and J. Boatwright (2005). Hypocenter locations in finite-source rupture models, *Bull. Seismol. Soc. Am.* **95,** 965–980.

Mai, P. M., P. Somerville, A. Pitarka, L. Dalguer, S. G. Song, G. Beroza, H. Miyake, and K. Irikura (2006). On scaling of fracture energy and stress drop in dynamic rupture models: Consequences for near-source ground motions, in *Earthquakes: Radiated Energy and the Physics of Faulting*, R. Abercrombie, A. McGarr, H. Kanamori, and G. Di Toro (Editors), Geophysical Monograph Series **170,** 283–293.

Marone, C. (1998). Laboratory-derived friction laws and their application to seismic faulting, *Ann. Revs. Earth Plan. Sci.* **26,** 643–696.

Marone, C., and C. H. Scholz (1988). The depth of seismic faulting and the upper transition from stable to unstable slip regimes, *Geophys. Res. Lett.* **15,** 621–624.

Marone, C. J., C. H. Scholz, and R. Bilham (1991). On the mechanics of earthquake afterslip, *J. Geophys. Res.* **96,** 8441–8452.

Oglesby, D. D., and S. M. Day (2002). Stochastic fault stress: Implications for fault dynamics and ground motion, *Bull Seismol. Soc. Am.* **92,** 3006–3021.

Okubo, P. G. (1989). Dynamic rupture modeling with laboratory-derived constitutive relations, *J. Geophys. Res.* **94,** 12321–12335.

Olsen, K. B., R. Madariaga, and R. Archuleta (1997). Three dimensional dynamic simulation of the 1992 Landers earthquake, *Science* **278,** 834–838.

Pitarka, A. (1999). 3D elastic finite-difference modeling of seismic motion using staggered grid with nonuniform spacing, *Bull. Seismol. Soc. Am.* **89,** 54–68.

Pitarka, A., S. Day, and L. Dalguer (2005). Investigation of shallow crustal weak zone effects on rupture dynamics of surface and subsurface faulting, *Proceedings and Abstracts Vol. XV, 2005 Southern California Earthquake Center (SCEC) Annual Meeting*, Palm Springs, California, 168.

Power, M., B. Chiou, N. Abrahamson, Y. Bozorgnia, T. Shantz, and C. Roblee (2008). An overview of the NGA project, *Earthq. Spectra* **24**, no. 1.

Ripperger, J., P. M. Mai, and J.-P. Ampuero (2008). Variability of near-field ground motion from dynamic earthquake rupture simulations, *Bull. Seismol. Soc. Am.* **98,** 1207–1228.

Shimamoto, T., and J. M. Logan (1981). Effects of simulated clay gouges on the sliding behavior of Tennessee sandstone, *Tectonophysics* **75,** 243–255.

Somerville, P. G. (2003). Magnitude scaling of the near fault rupture directivity pulse, *Phys. Earth Planet. Int.* **137,** 201–212.

Somerville, P. G., and A. Pitarka (2006). Differences in earthquake source and ground motion characteristics between surface and buried earthquakes, *Proc. of the Eighth National Conference on Earthquake Engineering*, San Francisco, California.

Somerville, P., K. Irikura, R. Graves, S. Sawada, D. J. Wald, N. Abrahmason, Y. Iwasaki, T. Kagawa, N. Smith, and A. Kowada (1999). Characterizing crustal earthquake slip models for the prediction of strong ground motion, *Seism. Res. Lett.* **70,** no. 1, 59–80.

URS Corporation
566 El Dorado St., Second Floor
Pasadena, California 91101
paul_somerville@urscorp.com
(A.P., P.G.S.)

Institute of Geophysics
ETH Hoenggerberg
CH-8093 Zurich, Switzerland
dalguer@tomo.ig.erdw.ethz.ch
(L.A.D.)

Dept. of Geological Sciences
San Diego State University
San Diego, California 92182
day@moho.sdsu.edu
(S.M.D.)

Ohsaki Research Institute
Shimizu Corporation
Japan
kazuo.dan@shimz.co.jp
(K.D.)

Manuscript received 21 July 2008